# Spin of valence-band holes in wurtzite semiconductors

A. Dargys*
*Semiconductor Physics Institute, A. Goštauto 11, LT-01108 Vilnius, Lithuania*
(Received 2 November 2004; revised manuscript received 1 March 2005; published 25 July 2005)

Spin polarization properties of a ballistic hole in wurtzite semiconductors are analyzed using the concept of spin surface. It is shown that, in general, the spin surface in a three-dimensional spin space has the shape of spheroid whose minor/major axis and orientation depend on a relative strength of the spin-orbit and crystal-field interactions as well as on the hole wave vector direction and length. Analytical expressions for the spin surfaces of heavy-mass, light-mass, and split-off bands were found for two experimentally important cases, when the hole wave vector is parallel and perpendicular to the hexagonal axis. For an arbitrary direction of the wave vector the numerical results are presented which show that the spin surface remains the spheroid in this case as well. However, the surface transforms to a line or sphere at small and large wave vectors. The properties of the spin surfaces are illustrated for valence band parameters of GaN, where the crystal field dominates in the band-edge splitting.

DOI: 10.1103/PhysRevB.72.045220 PACS number(s): 71.70.Ej, 72.25.Hg, 75.47.−m, 85.75.−d

## I. INTRODUCTION

Electron and hole spin properties in wide-band-gap semiconductors such as GaN, GaP, or ZnO are of great interest due to their potential application in spintronics, where the spin of a free carrier provides a new functionality in micro- and nanoelectronic devices.[1] In particular, high Curie temperature of the wide-gap semiconductors doped with magnetic impurities, the so-called ferromagnetic semiconductors,[2,3] makes these materials especially attractive as spin injectors, spin-polarized light emitters, optical switches, and modulators that can function at room temperature. The possibility to control the spin of the free charge carrier injected from a ferromagnetic semiconductor by external electric field, due Rashba[4,5] or interband tunneling[6–8] mechanisms, makes them also perspective materials for the spin transistor.[9,10]

The physical properties of spin usually are described by the polarization vector, which is defined as an average spin, $\mathbf{P}=\langle\chi|\boldsymbol{\sigma}|\chi\rangle/2$, of a particle in a state $|\chi\rangle$.[11] Here $\boldsymbol{\sigma}$ is the vectorial operator made up of three Pauli matrices. When $|\chi\rangle$ describes one of spin eigenstates, either up or down spin along the quantization axis $z$, then $\mathbf{P}$ reduces to a simple form: $\mathbf{P}=(P_x,P_y,P_z)=(0,0,\pm\frac{1}{2})$. If the spinor is in a superposition state, then, in general, all three Cartesian components of $\mathbf{P}$ will not be equal to zero. For nonrelativistic conduction band electrons in semiconductors the modulus of $\mathbf{P}$ is $|\mathbf{P}|=\frac{1}{2}$. By this reason only the direction of $\mathbf{P}$ will matter in the description of electron polarization properties.[11] In the case of valence band holes, as shown in Refs. 12 and 13, the information about spin direction is not complete. Due to strong spin-orbit interaction between valence subbands, $|\mathbf{P}|$ is not conserved. It depends on the hole wave vector $\mathbf{k}$ as well as on the band, where the hole has been excited, properties. In the case of the valence bands, the properties of the spin, as well as those of the total angular momentum, are better represented by spin surface which describes all possible $\mathbf{P}$'s in a three-dimensional spin space. For example, in Refs. 12 and 13 it was found that the spin surface of a heavy-mass hole in the elementary and $A_3B_5$ semiconductors is cigar-shaped with the symmetry axis being parallel to the hole wave vector. The origin of deviation from spherical shape comes from the noncommutativity of the spin (as well as of the total angular momentum) operator and valence band Hamiltonian. The first investigations[6–8] have shown that the concept of the spin surface is very useful in determining the initial conditions in the time-dependent Schrödinger equation and in explaining hole spin properties in an ultrafast spin switching dynamics in high electric fields. Also the concept of the spin surface can explain the anisotropy of spin injection from ferromagnetic semiconductors.[12]

In this paper the spin properties of holes in the wurtzite-type semiconductors, where apart from spin-orbit also crystal-field interaction comes into play, are considered. Due to the very complicated valence band structure of these semiconductors, the spin surfaces can be found by numerical methods only, if the hole propagates in an arbitrary direction. The paper shows that in spite of this complication, it appears possible to find analytical solutions in two important practical situations, namely, when the wave vector of a ballistic hole is either parallel or perpendicular to the crystal hexagonal axis. In the next section the properties of the wurtzite Hamiltonian in the standard basis are reviewed at first and the corresponding spin matrices are presented. In the subsequent section a unitary transformation matrix that connects basis wave functions in the standard and energy representation, where the parametrization of the wave function can be done easily, is constructed. The knowledge of the transformation matrix will allow us to find spin surfaces for all—heavy-mass, light-mass, and crystal-field split-off—energy bands of wurtzite-type semiconductors.

## II. HAMILTONIAN AND SPIN MATRICES

In wide-gap wurtzites the structure of the uppermost valence bands is determined by two competing mechanisms, the crystal-field interaction and spin-orbit interaction.[14–16] The hexagonal component of the crystal field in the wurtzites

 

is relatively large; as a result, all three valence bands—heavy-hole (HH), light-hole (LH), and crystal-field split-off (CH)—are separated by respective energy gaps. Incorporation of the hole wave vector usually is done by the $\mathbf{k}\cdot\mathbf{p}$ perturbation theory[17] or the invariant method.[14] Using the spherical harmonic representation given by the basis functions $Y_{pm}$,

$$|Y\rangle = (|Y_{11}\uparrow\rangle, |Y_{11}\downarrow\rangle, |Y_{10}\uparrow\rangle, |Y_{10}\downarrow\rangle, |Y_{1-1}\uparrow\rangle, |Y_{1-1}\downarrow\rangle)^T, \quad (1)$$

where up and down arrows indicate the hole spin state, one obtains the following effective-mass Hamiltonian matrix for a wurtzite-type valence band at the finite wave vector $\mathbf{k}$,[14–16,18]

$$\hat{H} = \begin{bmatrix} F & 0 & -H^* & 0 & K^* & 0 \\ 0 & G & \Delta & -H^* & 0 & K^* \\ -H & \Delta & \lambda & 0 & \Pi^* & 0 \\ 0 & -H & 0 & \lambda & \Delta & \Pi^* \\ K & 0 & \Pi & \Delta & G & 0 \\ 0 & K & 0 & \Pi & 0 & F \end{bmatrix}. \quad (2)$$

The components of (2) in the atomic units ($e=\hbar=m_0=1$) are given by

$$F = \Delta_1 + \Delta_2 + \lambda + \theta,$$

$$G = \Delta_1 - \Delta_2 + \lambda + \theta,$$

$$\lambda = [A_1 k_z^2 + A_2(k_x^2 + k_y^2)]/2,$$

$$\theta = [A_3 k_z^2 + A_4(k_x^2 + k_y^2)]/2,$$

$$K = A_5(k_x + ik_y)^2/2,$$

$$H = (iA_6 k_z/2 - A_7)(k_x + ik_y),$$

$$\Pi = (iA_6 k_z/2 + A_7)(k_x + ik_y),$$

$$\Delta = \Delta_3\sqrt{2}. \quad (3)$$

In the Hamiltonian (2), $k_z$ was chosen to be parallel to $c$ axis, i.e., to the crystallographic (0001) axis having the sixfold symmetry. The band parameter $A_7$ determines the spin splitting. If $A_7=0$, one can show that all bands become doubly (spin) degenerate. The eigenvalues of (2) and (3) give the dependence of band energies on the wave vector $\mathbf{k}$. Figure 1 shows HH, LH, and CH bands, when the wave vector is either perpendicular or parallel to the $c$ axis. The parameters of GaN (see Table I) were used in these and all subsequent numerical calculations. When $A_7=0$, a characteristic feature to be noted in Fig. 1(a) is the intersection of LH and CH bands at $\mathbf{k}$'s that correspond to thermal hole energies. Very strong nonparabolicity of the bands is observed at these energies if $A_7 \neq 0$. Thus, the coefficient $A_7$ takes into account the hole spin interaction that is relatively weak at all wave vectors except the region of LH and CH band crossing. Figure 1(a) also shows that at the crossing point ($k_t \approx 0.028$ Å$^{-1}$=0.28 nm$^{-1}$) the lifting of band degeneracy is

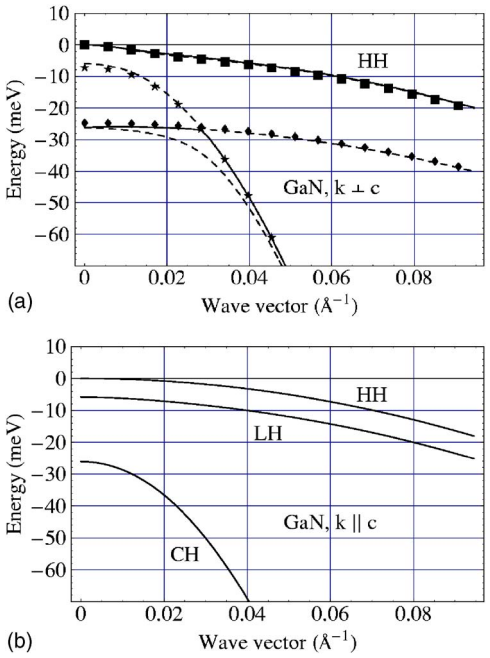


FIG. 1. (Color online) Valence band of wurtzite GaN when the hole wave vector $\mathbf{k}$ is (a) perpendicular and (b) parallel to $c$ axis. The points, which represent doubly degenerate bands, were calculated with the approximate formulas (9). The curves in (a) and (b) were calculated with the exact Hamiltonian (2). In (b) all energies are spin degenerate, while in (a) the spin degeneracy is lifted, however, the splitting of the HH band (solid curve) and of the next two bands (represented by upper dashed curve) are too small to be seen in the plot. In the approximate model represented by points in (a) the LH and CH bands intersect, while in the exact model the band crossing is absent. All energies were shifted down, so that at $\mathbf{k}=0$ the band edge of the HH band is at zero energy.

different for different bands. The valence band structure is determined by both the crystal-field and spin-orbit interactions. However, as we shall see, the deformation of spin surfaces comes from the spin-orbit interaction only.

In Ref. 18 it was shown that the Hamiltonian (2) can be block diagonalized, even when $A_7 \neq 0$, if new basis functions (in the following referred to as $v$ basis) are chosen:

$$|v_1\rangle = \alpha^*|Y_{11}\uparrow\rangle - \alpha|Y_{1-1}\downarrow\rangle,$$

$$|v_2\rangle = \beta|Y_{1-1}\uparrow\rangle - \beta^*|Y_{11}\downarrow\rangle,$$

$$|v_3\rangle = -\beta^*|Y_{10}\uparrow\rangle + \beta|Y_{10}\downarrow\rangle,$$

$$|v_4\rangle = \alpha^*|Y_{11}\uparrow\rangle + \alpha|Y_{1-1}\downarrow\rangle,$$

TABLE I. The effective-mass parameters for the valence band of wurtzite GaN: $\Delta_i$'s are in units of meV, $A_i$'s are in atomic units (or in units of $\hbar^2/m_0$) except for $A_7$ which is in units of eV Å$^{-1}$ (Ref. 18).

| $\Delta_1$ | $\Delta_2$ | $\Delta_3$ | $A_1$ | $A_2$ | $A_3$ | $A_4$ | $A_5$ | $A_6$ | $A_7$ |
|---|---|---|---|---|---|---|---|---|---|
| 21.2 | 3.61 | 3.61 | −7.21 | −0.440 | 6.66 | −3.46 | −3.40 | −4.9 | 0.0937 |

$$|v_5\rangle = \beta|Y_{1-1}\uparrow\rangle + \beta^*|Y_{11}\downarrow\rangle,$$

$$|v_6\rangle = -\beta^*|Y_{10}\uparrow\rangle + \beta|Y_{10}\downarrow\rangle, \tag{4}$$

where $\alpha=\exp(-i3\phi/2)\sqrt{2}$ and $\beta=\exp(-i\phi/2)\sqrt{2}$. The angle in the exponents is defined as $\phi=\tan^{-1}(k_x/k_y)$, where $k_x$ and $k_y$ are the wave vector components perpendicular to the $c$ axis. In (4), some of the terms have opposite sign to that used in Ref. 18. In the following it will be convenient to perform the transformation of all operators, including the Hamiltonian (2), to basis (4) using the following unitary matrix:

$$\hat{U} = \begin{bmatrix} \alpha^* & 0 & 0 & 0 & 0 & \alpha \\ 0 & -\beta^* & 0 & 0 & \beta & 0 \\ 0 & 0 & -\beta^* & \beta & 0 & 0 \\ \alpha^* & 0 & 0 & 0 & 0 & \alpha \\ 0 & \beta^* & 0 & 0 & \beta & 0 \\ 0 & 0 & \beta^* & \beta & 0 & 0 \end{bmatrix}. \tag{5}$$

Then in the new, block-diagonalized Hamiltonian $\hat{H}_{U,L}=\hat{U}\hat{H}\hat{U}^\dagger$ the upper $3\times3$ block $\hat{H}_U$ assumes the following form:

$$\hat{H}_U = \frac{1}{2}\begin{bmatrix} \varepsilon + 2(\Delta_1+\Delta_2) & A_5k_t^2 & -(2A_7+iA_6k_z)k_t \\ A_5k_t^2 & \varepsilon + 2(\Delta_1-\Delta_2) & -(2A_7+iA_6k_z)k_t + \sqrt{2}\Delta_3 \\ -(2A_7-iA_6k_z)k_t & -(2A_7-iA_6k_z)k_t + \sqrt{2}\Delta_3 & -A_2k_t^2 + A_1k_z^2 \end{bmatrix}, \tag{6}$$

where $\varepsilon=(A_2+A_4)k_t^2+(A_1+A_3)k_z^2$ and $k_t^2=k_x^2+k_y^2$. The lower block $\hat{H}_L$ can be obtained from $\hat{H}_U$, if the sign of $k_t$ is changed to the opposite. At $\mathbf{k}=0$, from $\hat{H}_U$ and $\hat{H}_L$ one finds that the energies at the band edges of CH, LH, and HH bands are expressed through $\Delta_i$'s only:

$$E_{\mathrm{CH0}} = \tfrac{1}{2}[(\Delta_1-\Delta_2) - \sqrt{8\Delta_3^2+(\Delta_1-\Delta_2)^2}],$$

$$E_{\mathrm{LH0}} = \tfrac{1}{2}[(\Delta_1-\Delta_2) + \sqrt{8\Delta_3^2+(\Delta_1-\Delta_2)^2}],$$

$$E_{\mathrm{HH0}} = \Delta_1+\Delta_2. \tag{7}$$

The parameter $\Delta_1$ determines the contribution of the crystal-field interaction, while $\Delta_2$ and $\Delta_3$ are responsible for spin-orbit interaction. In GaN, as Table I shows, $\Delta_1 \gg \Delta_2, \Delta_3$ and one has that $E_{\mathrm{CH0}}\approx 0$, $E_{\mathrm{HH0}}\approx E_{\mathrm{LH0}}\approx\Delta_1$. Thus, in GaN the heavy- and light-hole bands in the vicinity of $\mathbf{k}=0$ are nearly degenerate, while the crystal-field band is detached by energy $\approx\Delta_1$. In the next section the eigenvectors of the Hamiltonians $\hat{H}_U$ and $\hat{H}_L$ will be used to find the approximations to the unitary matrix that connects the $v$ basis with the energy basis.

Due to the small contribution of the spin splitting (coefficient $A_7$) as compared to other splitting mechanisms, in the analytical calculations $A_7$ will be neglected. Thus, one can assume that the hole is in one pair of the doubly degenerate energy bands (or nearly degenerate bands in case of numerical simulations), the wave function of which may be parametrized by a pair of variables. To calculate the hole spin surface when the hole with a given wave vector $\mathbf{k}$ is propagating in HH, LH, or CH degenerate bands, one must know $6\times6$ spin matrices $S_i$ (where $i=x,y$ or $z$) in one of the representations, i.e., in the energy, $Y$, or $v$ basis. The simplest form for $S_i$ is obtained in the $Y$ basis, since the components of the hole spin in this basis can be expressed through pure spin states. The spin matrices in this basis are expressed as a direct product of $3\times3$ unit matrix $I_{3\times3}$ and Pauli matrices $\sigma_i$:

$$S_i = I_{3\times3}\otimes\sigma_i/2. \tag{8}$$

Expression (8) shows that $6\times6$ hole spin matrices are block diagonal [see also the Appendix, where it is explicitly shown that the spin-orbit interaction is responsible for the noncommutativity of spin matrices (8) and Hamiltonian (2)]. In the following, the matrix (8) will be used to find spin surfaces when HH, LH, and CH band wave functions have been parametrized and transformed to a $Y$ basis.

## III. UNITARY TRANSFORMATION MATRICES

The simplest form of spin parametrized wave functions is in the energy representation, since band energies in this representation are degenerate or nearly degenerate as Fig. 1 shows. The transformation matrix that connects energy representation with $Y$ representation (1) will be calculated from the eigenvectors of $\hat{H}_U$ and $\hat{H}_L$ blocks. This can be done by a symbolic algebra package such as *Mathematica*. However, in this way calculated eigenvectors have been found too complicated to be of any practical use. By this reason below two special cases—when the wave vector is either perpendicular or parallel to the hexagonal $c$ axis—will be considered.

### A. $\mathbf{k}\perp c$ case

In this case $k_z=0$ and the transformation matrix is a function of the transverse wave vector, $k_t=\sqrt{k_x^2+k_y^2}$, only. As mentioned, we shall also assume that all bands are doubly degenerate, i.e., $A_7=0$. However, even under these simplifying conditions the eigenvalues and eigenvectors of $\hat{H}_{U,L}$ are still expressed through cubic roots and are rather complicated. The cubic roots reduce to quadratic if the band coefficient $\Delta_3$

is equated to zero. Thus, under the assumption that $k_z=0$, $A_7=0$, and $\Delta_3=0$, the bands have the following dispersion laws in the directions perpendicular to the $c$ axis:

$$E_{\mathrm{CH}\perp}=A_2k_t^2/2,$$

$$E_{\mathrm{LH}\perp}=[(A_2+A_4)k_t^2+2\Delta_1-s]/2,$$

$$E_{\mathrm{HH}\perp}=[(A_2+A_4)k_t^2+2\Delta_1+s]/2, \tag{9}$$

where $s=\sqrt{A_5^2k_t^4+4\Delta_2^2}$. The squares, diamonds, and stars in Fig. 1(a) show the dispersion curves described by Eqs. (9). It is seen that for GaN, except for the region where LH and CH bands cross, the points lie very close to curves calculated numerically with the initial Hamiltonian (2). At $k_t=0$, the band edges of the HH and LH bands with respect to the CH band are now, respectively, $\Delta_1+\Delta_2$ and $\Delta_1-\Delta_2$. Thus, the crystal-field and spin-orbit splitting in this approximation are described by two parameters, $\Delta_1$ and $\Delta_2$.

Using the eigenvectors of $\hat{H}_U$ and $\hat{H}_L$, now it is easy to find the unitary transformation matrix $T_\perp$ that transforms the initial Hamiltonian (2) to a diagonal form:

$$\hat{H}_{\mathrm{diag}}=T_\perp\hat{H}T_\perp^\dagger=\{E_{\mathrm{CH}\perp},E_{\mathrm{LH}\perp},E_{\mathrm{HH}\perp},E_{\mathrm{CH}\perp},E_{\mathrm{LH}\perp},E_{\mathrm{HH}\perp}\}. \tag{10}$$

The energies in the last expression show the order of the valence bands (9) in the resulting diagonalized Hamiltonian $\hat{H}_{\mathrm{diag}}$. The required unitary transformation matrix is

$$T_\perp=\begin{bmatrix}
0 & 0 & -\frac{e^{i\phi/2}}{\sqrt{2}} & \frac{e^{-i\phi/2}}{\sqrt{2}} & 0 & 0\\
-t^{(-)}e^{3i\phi/2} & -\frac{e^{i\phi/2}}{2r^{(+)}} & 0 & 0 & \frac{e^{-i\phi/2}}{2r^{(+)}} & t^{(-)}e^{-3i\phi/2}\\
t^{(+)}e^{3i\phi/2} & -\frac{e^{i\phi/2}}{2r^{(-)}} & 0 & 0 & \frac{e^{-i\phi/2}}{2r^{(-)}} & -t^{(+)}e^{-3i\phi/2}\\
0 & 0 & \frac{e^{i\phi/2}}{\sqrt{2}} & \frac{e^{-i\phi/2}}{\sqrt{2}} & 0 & 0\\
-t^{(-)}e^{3i\phi/2} & \frac{e^{i\phi/2}}{2r^{(+)}} & 0 & 0 & \frac{e^{-i\phi/2}}{2r^{(+)}} & -t^{(-)}e^{-3i\phi/2}\\
t^{(+)}e^{3i\phi/2} & \frac{e^{i\phi/2}}{2r^{(-)}} & 0 & 0 & \frac{e^{-i\phi/2}}{2r^{(-)}} & t^{(+)}e^{-3i\phi/2}
\end{bmatrix}, \tag{11}$$

where

$$r^{(\pm)}=\sqrt{s/(s\pm2\Delta_2)},$$

$$t^{(\pm)}=(s\pm2\Delta_2)/(2A_5k_t^2r^{(\mp)}). \tag{12}$$

Since $s$ and $\phi$ are functions of the transverse wave vector, the transformation matrix (11) depends on $k_t$, too. This produces the deformation of spin surfaces. This property was found in zinc-blende semiconductors, too.[12,13]

### B. k∥c case

Now the hole moves along the $c$ axis ($k_t=0$). In this case no approximations are needed to find the eigenvectors. Both Hamiltonians, $\hat{H}_U$ and $\hat{H}_L$, give the same dispersion laws:

$$E_{\mathrm{HH}\parallel}=\tfrac{1}{2}(A_1+A_3)k_z^2+\Delta_1+\Delta_2,$$

$$E_{\mathrm{CH}\parallel}=\tfrac{1}{4}(2A_1k_z^2+u-w),$$

$$E_{\mathrm{LH}\parallel}=\tfrac{1}{4}(2A_1k_z^2+u+w), \tag{13}$$

where

$$u=A_3k_z^2+2\Delta_1-2\Delta_2,$$

$$w=\sqrt{u^2+32\Delta_3^2}. \tag{14}$$

The dispersions (13) are exact and, therefore, they will coincide with those calculated numerically in Fig. 1(b) using the initial Hamiltonian (2). The unitary transformation matrix $T_\parallel$ that diagonalizes the Hamiltonian to form $\hat{H}_{\mathrm{diag}}=T_\parallel\hat{H}T_\parallel^\dagger=\{E_{\mathrm{CH}\parallel},E_{\mathrm{LH}\parallel},E_{\mathrm{HH}\parallel},E_{\mathrm{CH}\parallel},E_{\mathrm{LH}\parallel},E_{\mathrm{HH}\parallel}\}$ now is

$$T_{\parallel} = \begin{bmatrix} 0 & -\frac{u-w}{2v^{(-)}} & -\frac{4\Delta_3}{s^{(-)}} & \frac{4\Delta_3}{s^{(-)}} & \frac{u-w}{2v^{(-)}} & 0 \\ 0 & -\frac{u+w}{2v^{(+)}} & -\frac{4\Delta_3}{s^{(+)}} & \frac{4\Delta_3}{s^{(+)}} & \frac{u+w}{2v^{(+)}} & 0 \\ \frac{1}{\sqrt{2}} & 0 & 0 & 0 & 0 & -\frac{1}{\sqrt{2}} \\ 0 & \frac{u-w}{2v^{(-)}} & \frac{4\Delta_3}{s^{(-)}} & \frac{4\Delta_3}{s^{(-)}} & \frac{u-w}{2v^{(-)}} & 0 \\ 0 & \frac{u+w}{2v^{(+)}} & \frac{4\Delta_3}{s^{(+)}} & \frac{4\Delta_3}{s^{(+)}} & \frac{u+w}{2v^{(+)}} & 0 \\ \frac{1}{\sqrt{2}} & 0 & 0 & 0 & 0 & \frac{1}{\sqrt{2}} \end{bmatrix}, \tag{15}$$

where

$$v^{(\pm)} = \sqrt{u(u \pm w) + 32\Delta_3^2},$$

$$s^{(\pm)} = \sqrt{(u \pm w)^2 + 32\Delta_3^2}. \tag{16}$$

Since the dispersion laws (13) are exact the transformation matrix (15) is exact, too.

## IV. SPIN SURFACES

The spin surface describes all possible locations of the end of average spin vector $\langle \mathbf{S} \rangle_n = (\langle S_x \rangle_n, \langle S_y \rangle_n, \langle S_z \rangle_n)$, when the wave function $|f_n(\mathbf{k})\rangle$ of the doubly degenerate $n$th band, HH, LH, or SH, is parametrized. The average hole spin is

$$\langle \mathbf{S} \rangle_n = \langle f_n(\mathbf{k}) | \mathbf{S} | f_n(\mathbf{k}) \rangle, \tag{17}$$

where the components $S_{x,y,z}$ of the spin operator $\mathbf{S}$ are given by Eq. (8). The expression for $|f_n(\mathbf{k})\rangle$ has very complicated form if one tries to represent it through the energy gaps and conduction-valence band masses of the considered semiconductor.[19–21] However, the parametrized form of $|f_n(\mathbf{k})\rangle$ is very simple in the energy representation, where the spinor is represented as a plane wave propagating in the $n$th energy band and having the wave vector $\mathbf{k}$. The polarization of the hole described by this spinor may be pointing to arbitrary direction and is determined by concrete values of the parameters in the spinor. The respective spinors $|\psi_n\rangle$ in the energy representation can be related to the $Y$ representation given by (1), if unitary transformation matrix $T$ between the two representations is known:

$$|f_n(\mathbf{k})\rangle = T(\mathbf{k}) |\psi_n\rangle. \tag{18}$$

The needed transformation matrices for holes perpendicular and parallel to $c$ axis wave vector $\mathbf{k}$ are given, respectively, by Eqs. (11) and (15).

### A. $\mathbf{k} \perp c$ case

*CH band*. In the energy representation the spinor of the CH band that conforms with the band order in the Hamiltonian (10) is assumed to have the following parametrized form:

$$|\psi\rangle_{\mathrm{CH}\perp} = (\cos\theta, 0, 0, \sin\theta e^{i\varphi}, 0, 0). \tag{19}$$

After the transformation of (19) to the $Y$ representation, $|f(\mathbf{k})\rangle_{\mathrm{CH}\perp} = T_{\perp}^{\dagger}(\mathbf{k}) |\psi\rangle_{\mathrm{CH}\perp}$, the spin polarization (17) is found to be

$$\begin{aligned} \langle \mathbf{S} \rangle_{\mathrm{CH}\perp} = \langle f | \mathbf{S} | f \rangle_{\mathrm{CH}\perp} = -\tfrac{1}{2}(&\cos 2\theta \cos\phi \\ &- \sin 2\theta \sin\varphi \sin\phi, \cos 2\theta \sin\phi \\ &+ \sin 2\theta \sin\varphi \cos\phi, \sin 2\theta \cos\varphi), \end{aligned} \tag{20}$$

where $\phi = \tan^{-1}(k_y/k_x)$ is the azimuthal angle of the transverse wave vector. The square of $\langle \mathbf{S} \rangle_{\mathrm{CH}\perp}$ is independent of the parameters $\theta$ and $\varphi$ as well as of the azimuthal angle $\phi$ and equals $\frac{1}{4}$. Thus, for the CH band the spin surface is the sphere of radius $\frac{1}{2}$ and all directions of the spin are equivalent under the approximations used: $A_7 = 0$ and $\Delta_3 = 0$. The azimuthal angle $\phi$ in Eq. (20) can be set to zero, since all transverse wave vectors are equivalent. If one wants to preserve the initial direction of the spin polarization given by Eq. (20), the values of the parameters $\theta$ and $\varphi$ must be shifted by a constant value.

The numerical calculations using valence band parameters of GaN show that the true spin surface of the CH band slightly deviates from the spherical shape. Analysis shows that it has a form of the ellipsoid of rotation (spheroid) rather than that of the sphere. The points in Fig. 2(a) show the dependence of the minor and major axes of the CH spheroid as functions of $k_t$. The largest deviation is observed in the vicinity of crossing of the CH and LH bands, where the spectrum also suffers the largest deviation as seen in Fig. 1(a). At smaller wave vectors the agreement between exact and approximate calculations is much better. At large wave vectors, $k_t > 0.4\ \mathrm{nm}^{-1}$, the spin surface is very close to sphere.

*LH band*. The parametrized form of the light-mass spinor is

$$|\psi\rangle_{\mathrm{LH}\perp} = (0, \cos\theta, 0, 0, \sin\theta e^{i\varphi}, 0). \tag{21}$$

The average Cartesian components of the hole spin now have a more complex form:

$$\begin{aligned} \langle \mathbf{S} \rangle_{\mathrm{LH}\perp} &= \langle f | \mathbf{S} | f \rangle_{\mathrm{LH}\perp} \\ &= \left( \frac{A_5 k_t^2 (\cos 2\theta \cos\phi + \sin 2\theta \sin\varphi \sin\phi)}{2\sqrt{A_5^2 k_t^4 + 4\Delta_2^2}}, \right. \\ &\quad \frac{A_5 k_t^2 (\cos 2\theta \sin\phi - \sin 2\theta \sin\varphi \cos\phi)}{2\sqrt{A_5^2 k_t^4 + 4\Delta_2^2}}, \\ &\quad \left. \frac{\sin 2\theta \cos\varphi}{2} \right). \end{aligned} \tag{22}$$

As the parameters $\theta$ and $\varphi$ are varied, the end of the average spin (22) in the spin space draws the spheroid, whose rotation axis is parallel to $c$ axis. In the limiting case of small wave vectors, $k_t \to 0$, the spin surface reduces to a line perpendicular to $k_t$ and parallel to $c$ axis: $\langle \mathbf{S}(k_t = 0) \rangle_{\mathrm{LH}\perp}$

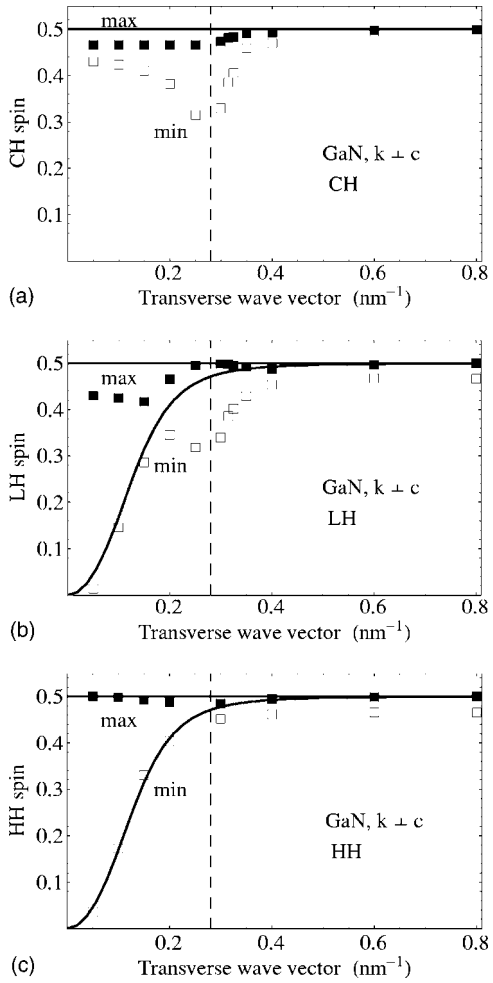


FIG. 2. Dependence of the minor (min) and major (max) axes of the spin spheroids of (a) crystal-field split-off hole, (b) light-hole, and (c) heavy-hole bands on the magnitude of transverse wave vector. Points: exact calculations. Lines: approximations by formulas (20) and (22). The vertical dashed line shows the wave vector ($k_t$ =0.28 nm$^{-1}$) at which LH and CH band crossing takes place.

$=\frac{1}{2}(0,0,\sin 2\theta\cos\varphi)$. Thus, at small wave vectors $k_t$ the light-hole spin will be perpendicular to the hole propagation direction. In the opposite limit, when $k_t$ is large, the spin surface (22) reduces to a sphere of radius $\frac{1}{2}$. At the intermediate $k_t$ values the spin surface is spheroid. From Eq. (22) it follows that the distance from the center to any point on the spheroid surface is

$$|\langle \mathbf{S}\rangle_{\mathrm{LH}\perp}| = \frac{1}{2}\sqrt{\frac{A_5^2k_t^4 + 4\Delta_2^2\sin^2 2\theta\cos^2\varphi}{A_5^2k_t^4 + 4\Delta_2^2}}, \qquad (23)$$

from which one finds that the major axis ($\theta=\pi/4, \varphi=0$) of the spheroid is $\frac{1}{2}$, while the minor axis ($\theta=0$) is $\frac{1}{2}(1+(2\Delta_2/A_5k_t^2)^2)^{-1/2}$. At the CH and LH band crossing, $k_t \approx 0.28$ nm$^{-1}$, this formula gives that the minor axis is $\approx 0.47$ for parameters of GaN, i.e., the spin surface is close to a sphere. The exact calculations give that the deviation from the spherical shape at the band crossing point, in fact, is larger [see points in Fig. 2(b)]. However, numerical and analytical calculations give that at large wave vectors the spin surface is close to a sphere and at small wave vectors it can be approximated by line parallel to $c$ axis.

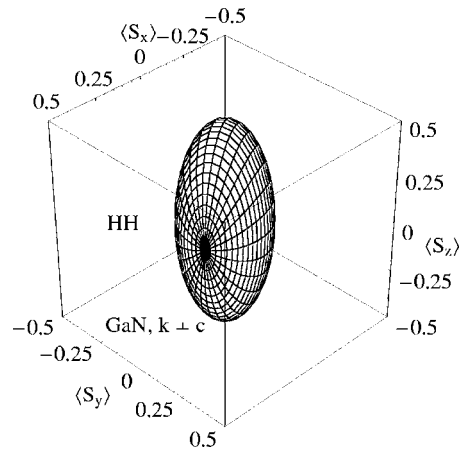


FIG. 3. Heavy-hole spin surface represented by geodesic lines at the transverse wave vector $k_t$=0.113 nm$^{-1}$ and $\phi=\pi/8$. The rotation axis of the spheroid is parallel to $\langle S_z\rangle$ component.

*HH band*. The parametrized form of the heavy-mass band wave function is

$$|\psi\rangle_{\mathrm{HH}\perp} = (0,0,\cos\theta,0,0,\sin\theta e^{i\varphi}). \qquad (24)$$

Analytical calculations with (24) have shown that the overall shape of the heavy-hole spin surface is similar to that of the light hole, Eq. (22). Comparison with the exact numerical calculations gives that the formula (22) now approximates the spin surface fairly well, Fig. 2(c). Figure 3 illustrates the full form of the heavy-hole spin surface at the small magnitude of the wave vector, $k_t$=0.113 nm$^{-1}$. It is an ellipsoid of rotation with the major axis parallel to $\langle S_z\rangle$. Here it should be remembered that the shape of the spin surface is invariant to a particular form of the parametrization of the spinor used to vizualize the surface. Different parametrization schemes will give different sets of the geodesic lines that run over the spin surface and different locations of poles where the geodesic lines meet. In Fig. 3 the poles meet on the sides of the spheroid rather than on the $\langle S_z\rangle$ axis as one would expect. To have the poles on the $\langle S_z\rangle$ axis a different parametrization scheme should be selected. If the azimuthal direction $\phi$ of the transverse wave vector $\mathbf{k}_t$ is changed, the pattern of the geodesic lines in Fig. 3 will rotate around the $\langle S_z\rangle$ axis, however the shape of the spin surface, as it should be, will remain invariant. Therefore, it is safe to set $\phi=0$ in the geodesic line formula (22). From what has been said one can conclude that the spin surface represents an intrinsic property of the hole spin and that the parametrization and geodesic lines only make it visible.

### B. k∥$c$ case

*HH band*. The simplest expression for the spin surface in this case is for heavy-mass holes. Using the parametrized form of the wave function $|\psi\rangle_{\mathrm{HH}\parallel}$, which coincides with $|\psi\rangle_{\mathrm{HH}\perp}$, one finds that the spin surface is represented by the line

$$\langle \mathbf{S} \rangle_{\mathrm{HH}\|} = \tfrac{1}{2}(0,0,\sin 2\theta \cos \varphi). \tag{25}$$

Since the transformation matrix (15) is exact, the formula (25) is exact, too. Thus, the heavy hole polarization is always parallel to $k_z$ and lies in the range from $-\frac{1}{2}$ to $\frac{1}{2}$, i.e., in this case independent of $\theta$ and $\varphi$ values one has $\langle \mathbf{S} \rangle_{\mathrm{HH}\|} \| k_z \| c$. A similar property was found for heavy-mass holes in elementary and $A_3B_5$ compounds.[12] As explained in Ref. 12, this property may be responsible for the high anisotropy of the spin injection efficiency from ferromagnetic to pure semiconductor.

*CH band*. For the crystal-field split-off band the calculations give the following spin polarization,

$$\langle \mathbf{S} \rangle_{\mathrm{CH}\|} = \frac{1}{2w(u-w)} \left( 16\Delta_3^2 \cos 2\theta, 16\Delta_3^2 \sin 2\theta \sin \varphi, \frac{[(u-w)^2 + 32\Delta_3^2][w(u-w) + 32\Delta_3^2]}{2w(-u+w)} \sin 2\theta \cos \varphi \right), \tag{26}$$

where the functions $u$ and $w$ were defined by Eqs. (14). In the limit $k_z \to 0$, the components of (26) reduce to

$$\langle \mathbf{S}(k_z = 0) \rangle_{\mathrm{CH}\|} = -\left( \frac{2\Delta_3^2 \cos 2\theta}{\delta(-\Delta_1 + \Delta_2 + \delta)}, \frac{2\Delta_3^2 \sin 2\theta \sin \varphi}{\delta(-\Delta_1 + \Delta_2 + \delta)}, \frac{(\Delta_1 - \Delta_2)\sin 2\theta \cos \varphi}{2\delta} \right), \tag{27}$$

where $\delta = \sqrt{(\Delta_1 - \Delta_2)^2 + 8\Delta_3^2}$. For parameters of GaN Eq. (27) gives

$$\langle \mathbf{S}(k_z = 0) \rangle_{\mathrm{CH}\|} = -(0.466 \cos 2\theta, 0.466 \sin 2\theta \sin \varphi, 0.432 \sin 2\theta \cos \varphi).$$

Thus, at small wave vectors the spin surface appears to be close to a sphere. However, in the opposite limit, when $k_z \to \infty$, the spin components describe a line-shaped surface: $\langle \mathbf{S}(k_z = \infty) \rangle_{\mathrm{CH}\|} = -\frac{1}{2}(0,0,\sin 2\theta \cos \varphi)$.

*LH band*. The parametrized wave function $|\psi\rangle_{\mathrm{LH}\|} = (0, \cos\theta, 0, 0, \sin\theta e^{i\varphi}, 0)$ gives the following average spin:

$$\langle \mathbf{S} \rangle_{\mathrm{LH}\|} = \frac{1}{2[u(u+w) + 32\Delta_3^2]} (-16\Delta_3^2 \cos 2\theta, -16\Delta_3^2 \sin 2\theta \times \sin \varphi, u(u+w) \sin 2\theta \cos \varphi). \tag{28}$$

In the above expression it was assumed that $\phi = 0$. In the limit of small wave vectors, $k_z \to 0$, Eq. (28) reduces to

$$\langle \mathbf{S}(k_z = 0) \rangle_{\mathrm{LH}\|} = \left( -\frac{2\Delta_3^2 \cos 2\theta}{8\Delta_3^2 + (\Delta_1 - \Delta_2)(\Delta_1 - \Delta_2 + \delta)}, -\frac{2\Delta_3^2 \sin 2\theta \sin \varphi}{8\Delta_3^2 + (\Delta_1 - \Delta_2)(\Delta_1 - \Delta_2 + \delta)}, \frac{(\Delta_1 - \Delta_2)\sin 2\theta \cos \varphi}{2\delta} \right). \tag{29}$$

For GaN parameters Eq. (29) gives a cigar-shaped spin surface:

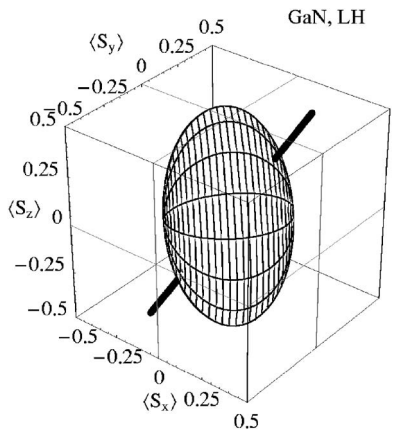


FIG. 4. Spin surface of the light-hole band at the wave vector magnitude $|\mathbf{k}| = 0.6\ \mathrm{nm}^{-1}$. The line shows the direction of $\mathbf{k}$ which makes an angle of 36° with the $c$ axis.

$$\langle \mathbf{S}(k_z = 0) \rangle_{\mathrm{LH}\|} = (-0.034 \cos 2\theta, -0.034 \sin 2\theta \sin \varphi, 0.432 \sin 2\theta \cos \varphi).$$

At large wave vectors, $k_z \to \infty$, Eq. (28) reduces to a formula for the line-shaped spin surface:

$$\langle \mathbf{S}(k_z = \infty) \rangle_{\mathrm{LH}\|} = \tfrac{1}{2}(0,0,\sin 2\theta \cos \varphi). \tag{30}$$

Thus, for light holes the spin surface is strongly elongated along the $c$ axis for all wave vector magnitudes.

### C. Arbitrary direction

For an arbitrary direction of $\mathbf{k}$ the spin surfaces can be calculated by numerical methods only. In this paper the transformation matrix at a fixed value of $\mathbf{k}$ was constructed from numerical eigenvectors of the initial Hamiltonian (2) using the singular value decomposition.[22] Since the decomposition is meaningful for positive eigenvalues only, before the decomposition the spectrum of the Hamiltonian was shifted accordingly and its sign was changed to opposite. Figure 4 shows the spin surface of the light hole when the wave vector makes 36° with the hexagonal axis. A characteristic feature is that the rotation axis of the spheroid now makes an angle with the wave vector shown by the straight line in the figure. A closer inspection will reveal that the rotation axis is slightly off from the $\langle S_z \rangle$ axis. To be sure that the spin surface indeed remains an ellipsoid of rotation, in Fig. 5 there is plotted the dependence of the radius $|\langle \mathbf{S} \rangle_{\mathrm{LH}}|$ on the counting number of the points through which the geodesic lines were drawn in Fig. 4. The parameter $\theta$ changes fastest and $\varphi$ changes slowest. The variation of $\theta$ at fixed $\varphi$ generates all geodesic lines that go through two poles on the surface. From the regularities in Fig. 5 it should be clear that the maximum and minimum values of $|\langle \mathbf{S} \rangle_{\mathrm{LH}}|$ correspond to the major and minor axes of the spheroid. Of course, different parametrization schemes will result in different geodesic line patterns drawn in Figs. 4 and 5; however, the overall shape of the spin surface will remain invariant. Figure 6 shows the dependence of the minor and major axes of the LH spin surface on the angle between the wave vector,

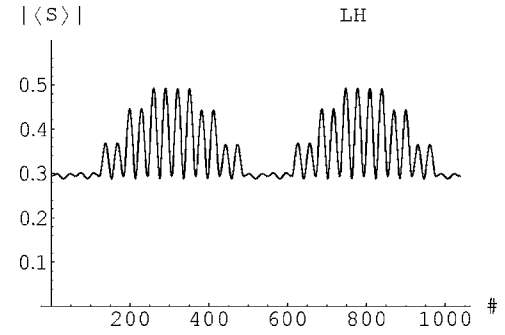


FIG. 5. Dependence of the spheroid radius in Fig. 4 on the point number # in the trajectory running over the surface, or equivalently on the parameter $\theta$ and $\varphi$ values, at $|\mathbf{k}|=0.6$ nm$^{-1}$. The parameter $\theta$ varies fastest while $\varphi$ varies slowest. The largest and smallest values of $|\langle \mathbf{S} \rangle_{\mathrm{LH}}|$ give, respectively, minor and major axes of the spheroid.

$|\mathbf{k}|=0.6$ nm$^{-1}$, and the quantization axis. The extreme values, 0° and 90°, correspond to the parallel and perpendicular wave vectors considered earlier. It is seen that independent of the direction of $\mathbf{k}$ the major axis is always equal to $\frac{1}{2}$, while the minor axis increases with angle. Exactly the same behavior was observed for HH band spin surface.

## V. DISCUSSION AND CONCLUSIONS

The numerical and analytical calculations show that in wurtzite-type semiconductors the spin surfaces, in general, are spheroids for all three valence bands. In the limit of large and small wave vector $\mathbf{k}$ the surface of a particular band may be spherical or reduce to a line. The nonsphericity of surfaces is associated with a spin-orbit interaction and noncommutativity of the wurtzite Hamiltonian with the spin matrix (Appendix). If band parameters $\Delta_2$ and $\Delta_3$, which are responsible for the spin-orbit interaction, are equated to zero, then similar calculations give that the spin surfaces of all three valence bands are represented by spheres.

In GaN the spin surface of the CH band was found to be spherical, or close to spherical. This property comes from the large crystal-field interaction in this material. The largest deviation from the sphericity was found in the vicinity of the crossing point of the CH and LH bands. Since the crystal-field splitting is determined by parameter $\Delta_1$, the spin surface will be more symmetrical the stronger the inequality $\Delta_1 > \Delta_2$, $\Delta_3$ is satisfied.

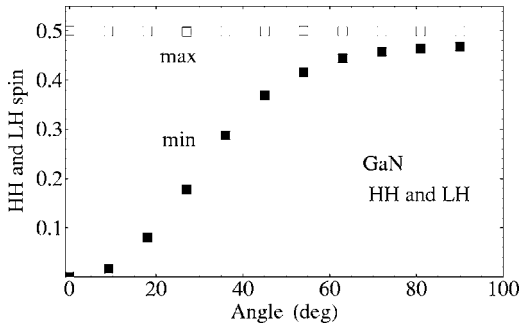


FIG. 6. Minor (min) and major (max) axes of the heavy- and light-hole spin surfaces as a function of the angle between the hole wave vector $\mathbf{k}$ and the hexagonal $c$ axis. $|\mathbf{k}|=0.6$ nm$^{-1}$.

The shape of spin surfaces in heavy- and light-mass bands is determined by parameters $\Delta_2$ and $\Delta_3$. At small $\mathbf{k}$'s the surfaces are cigar- and or even line-shaped. For larger wave vectors (beyond LH and SH band crossing) they transform to a sphere. However, there is one exception from this rule: the spin of the heavy-mass hole that propagates along the $c$ axis, as follows from numerical and exact calculations, is line shaped for all magnitudes of $k_z$. The exact formulas (25)–(27) in this case can serve as a reference in a numerical simulation. In the opposite case, when $\mathbf{k} \perp c$, due to band crossing, only approximate calculations are possible. Strong disturbance of spin surfaces is observed in the region of band crossing due to the mixing of four energy bands. The distortion mainly comes from interaction of LH and SH spin surfaces, the shapes of which at $\mathbf{k}=0$ are different as seen in Figs. 2(a) and 2(b). However, far away from the crossing point both surfaces regain the spherical shape.

When $\mathbf{k} \perp c$ the degeneracy of heavy, light, and crystal-field holes, in general, is lifted. The resulting small energy difference $\delta E_n = E_{n1} - E_{n2}$, where $n$=HH, LH, or CH, is known as spin splitting. A linear combination of spin eigenstates [see, for example, Eqs. (21) and (24)] used in constructing the spin surface gives small and slow oscillations of the hole energy and level population with the cyclic frequency $\delta E_n/\hbar$ and, as a consequence, a synchronous precession of the spin on the spin surface. This situation is very similar to that observed in EPR and NMR experiments,[23] where the superposition of two spin-split eigenstates of the electron or nucleus immersed in a dc magnetic field is achieved by applying an additional pulse of ac magnetic field in the perpendicular direction. Due to superposition, the spin precession in the latter case occurs around a dc magnetic field on the spherical spin surface synchronously with the energy oscillations. The angle of precession depends on the strength of mixing of up and down spin states. In our case the splitting of the HH, LH, or SH band is equivalent to some effective dc magnetic field which, however, has a local character, since the magnitude of the splitting $\delta E_n$ depends on the hole wave vector $\mathbf{k}$. The knowledge of the properties of spin surfaces allows one to determine the effective magnetic field in spintronic devices. More importantly, since the spin surface represents all possible spin polarizations of the ballistic hole, one can easily visualize the trajectories of the polarization vector on the spin surface under coherent control of the superposition of the spin states. Thus, with the help of the spin surface one can find a correspondence between the dynamics of the hole spin in the Hilbert space and that in the physical space. Recently, the spin surfaces were used in solving a difficult problem of hole spin relaxation due to phonon-induced intravalence and intervalence transitions in $p$-type semiconductors.[24] The shape of the spin surface, in general, may depend on spin splitting strength $\delta E_n$, especially when $\delta E_n$ is large. In Ref. 12 it was found that in $A_3B_5$ compounds the pure (i.e., without influence of band crossing) spin splitting $\delta E_n$ has negligible effect on the shape of the spin surface.

In Ref. 25 the 14-fold anisotropy of electrical spin injection efficiency between spin directions perpendicular and

parallel to hole current flow has been observed in ferromagnet-semiconductor heterostructures $Ga_{1-x}Mn_xAs$/GaAs with $x=0.045$ or 0.035. The experimentally detected anisotropy can be easily explained[12] with the help of a nonspherical (cigar-shaped) spin surface that is characteristic of heavy holes in $A_3B_5$ compounds. When the injected spin is parallel to the heavy-hole wave vector, the injected hole can propagate freely in GaAs; however, when the spin is perpendicular to **k** the hole cannot propagate, since the orthogonal configuration of the spin and wave vector is forbidden. By the same reasoning the spin injection anisotropy into GaN and similar compounds is expected, too, because, as follows from this paper, the spin surfaces in this material in general case are not spherical.

In conclusion, using parametrized spinors that represent individual valence band branches, the paper shows that, in general, the hole spin surfaces in the wurtzite-type semiconductors are spheroids. At small and large wave vectors the surfaces may reduce to a sphere or a line; as a consequence, the anisotropy of spin injection in these materials is predicted.

## APPENDIX: SPIN AND HAMILTONIAN COMMUTATION RELATIONS

In the basis (1), the Cartesian components $i=x,y,z$ of the spin matrix **S** are

$$S_i=\frac{1}{2}\begin{bmatrix}\sigma_i & 0 & 0\\ 0 & \sigma_i & 0\\ 0 & 0 & \sigma_i\end{bmatrix}, \tag{A1}$$

where $\sigma_i$'s are Pauli matrices

$$\sigma_x=\begin{bmatrix}0 & 1\\ 1 & 0\end{bmatrix},\quad \sigma_y=\begin{bmatrix}0 & -i\\ i & 0\end{bmatrix},\quad \sigma_z=\begin{bmatrix}1 & 0\\ 0 & -1\end{bmatrix}. \tag{A2}$$

The square of the matrix **S** is diagonal,

$$\mathbf{S}^2=S_x^2+S_y^2+S_z^2=\tfrac{3}{4}, \tag{A3}$$

therefore the operator $\mathbf{S}^2$ commutes with the Hamiltonian (2). However, the individual components of **S** do not commute with the Hamiltonian. The respective commutators are

$$[H,S_x]=\frac{1}{\sqrt{2}}\begin{bmatrix}0 & \Delta_2\sqrt{2} & -\Delta_3 & 0 & 0 & 0\\ -\Delta_2\sqrt{2} & 0 & 0 & \Delta_3 & 0 & 0\\ \Delta_3 & 0 & 0 & 0 & -\Delta_3 & 0\\ 0 & -\Delta_3 & 0 & 0 & 0 & \Delta_3\\ 0 & 0 & \Delta_3 & 0 & 0 & -\Delta_2\sqrt{2}\\ 0 & 0 & 0 & -\Delta_3 & \Delta_2\sqrt{2} & 0\end{bmatrix}, \tag{A4}$$

$$[H,S_y]=\frac{i}{\sqrt{2}}\begin{bmatrix}0 & -\Delta_2\sqrt{2} & \Delta_3 & 0 & 0 & 0\\ -\Delta_2\sqrt{2} & 0 & 0 & -\Delta_3 & 0 & 0\\ \Delta_3 & 0 & 0 & 0 & \Delta_3 & 0\\ 0 & -\Delta_3 & 0 & 0 & 0 & -\Delta_3\\ 0 & 0 & \Delta_3 & 0 & 0 & \Delta_2\sqrt{2}\\ 0 & 0 & 0 & -\Delta_3 & \Delta_2\sqrt{2} & 0\end{bmatrix}, \tag{A5}$$

$$[H,S_z]=\sqrt{2}\begin{bmatrix}0 & 0 & 0 & 0 & 0 & 0\\ 0 & 0 & \Delta_3 & 0 & 0 & 0\\ 0 & -\Delta_3 & 0 & 0 & 0 & 0\\ 0 & 0 & 0 & 0 & \Delta_3 & 0\\ 0 & 0 & 0 & -\Delta_3 & 0 & 0\\ 0 & 0 & 0 & 0 & 0 & 0\end{bmatrix}. \tag{A6}$$

The commutators are independent of the hole wave vector. They are equal to zero when the spin-orbit interaction is absent: $\Delta_2=\Delta_3=0$.

*Electronic address: dargys@pfi.lt

[1] I. Žutić, J. Fabian, and S. Das Sarma, Rev. Mod. Phys. **76**, 323 (2004).
[2] S. J. Pearton, C. R. Abernathy, M. E. Overberg, G. T. Thaler, D. P. Norton, N. Theodoropoulou, A. F. Hebard, Y. D. Park, F. Ren, J. Kim, and L. A. Boatner, J. Appl. Phys. **93**, 1 (2003).
[3] W. Prellier, A. Fauchet, and B. Mercey, J. Phys.: Condens. Matter **15**, R1583 (2003).
[4] Y. A. Bychkov and E. I. Rashba, Pis'ma Zh. Eksp. Teor. Fiz. **39**, 66 (1984) [JETP Lett. **39**, 78 (1984)].
[5] W. Zawadzki and P. Pfeffer, Semicond. Sci. Technol. **19**, R1 (2004).
[6] A. Dargys, Phys. Rev. B **70**, 125207 (2004).
[7] A. Dargys, IEEE J. Sel. Top. Quantum Electron. **10**, 155 (2004).
[8] A. Dargys, Acta Phys. Pol. A **107**, 46 (2005).
[9] S. Datta and B. Das, Appl. Phys. Lett. **56**, 665 (1990).
[10] A. Bournel, V. Delmovly, P. Dollfus, G. Tremblay, and P. Hesto, Physica E (Amsterdam) **10**, 86 (2001).
[11] J. Kessler, *Polarized Electrons* (Springer-Verlag, Berlin, 1985), Chap. 2.
[12] A. Dargys, Phys. Status Solidi B **241**, 2954 (2004).
[13] A. Dargys, Phys. Status Solidi B **241**, 145 (2004).
[14] G. L. Bir and G. E. Pikus, *Symmetry and Strain-Induced Effects in Semiconductors* (Wiley, New York, 1974), Chap. 5.
[15] S. L. Chuang and C. S. Chang, Phys. Rev. B **54**, 2491 (1996).
[16] D. Fritsch, H. Schmidt, and M. Grundmann, Phys. Rev. B **67**, 235205 (2003).
[17] E. O. Kane, in *Handbook on Semiconductors*, edited by W. Paul (North-Holland, Amsterdam, 1982), Vol. 1, pp. 193–217.
[18] G. B. Ren, Y. M. Liu, and P. Blood, Appl. Phys. Lett. **74**, 1117 (1999).
[19] E. O. Kane, J. Phys. Chem. Solids **1**, 249 (1957).

[20] M. Tiersten, IBM J. Res. Dev. **5**, 122 (1961).
[21] F. Szmulowicz and F. L. Madarasz, Phys. Rev. B **26**, 2101 (1982).
[22] G. H. Golub and C. F. Van Loan, *Matrix Computations* (The John Hopkins University Press, Baltimore, 1989), Chap. 8.
[23] T. C. Farrar and E. D. Becker, *Pulse and Fourier NMR. Introduction to Theory and Methods* (Academic Press, New York, 1971).
[24] A. Dargys, Semicond. Sci. Technol. **20**, 733 (2005).
[25] D. K. Young, E. Johnston-Halperin, D. D. Awschalom, Y. Ohno, and H. Ohno, Appl. Phys. Lett. **80**, 1598 (2002).